

# Quiescent times in $\gamma$ -ray bursts: II. Dormant periods in the central engine?

Enrico Ramirez-Ruiz, Andrea Merloni and Martin J. Rees

*Institute of Astronomy, Madingley Road, Cambridge, CB3 0HA*

## ABSTRACT

Within the framework of the internal-external shocks model for  $\gamma$ -ray bursts, we study the various mechanisms that can give rise to quiescent times in the observed  $\gamma$ -ray light-curves. In particular, we look for the signatures that can provide us with evidence as to whether or not the central engine goes dormant for a period of time comparable to the duration of the gaps. We show that the properties of the prompt  $\gamma$ -ray and X-ray emission can in principle determine whether the quiescent episodes are due to a modulated relativistic wind or a switching off of the central engine. We suggest that detailed observations of the prompt afterglow emission from the reverse shock will strongly constrain the possible mechanisms for the production of quiescent times in  $\gamma$ -ray bursts.

**Key words:** Gamma-rays: bursts – stars: supernovae – X-rays: sources

## 1 INTRODUCTION

The origin of  $\gamma$ -ray bursts (GRBs) has been one of the great unsolved mysteries in high-energy astrophysics for almost 30 years. The recent discovery of fading sources at X-ray (Costa et al. 1997) and optical (van Paradijs et al. 1997) wavelengths has established that GRBs lie at cosmological distances, making them the most luminous events known in the Universe. During their brief duration, their photon luminosities exceed by many orders of magnitude the most extreme output from any active galactic nucleus. However, the total energy budget needed to produce a GRB is not beyond the scope of some other phenomena encountered in astrophysics.

The two most popular models to explain GRBs are the coalescence of two compact objects such as black holes or neutron stars (Lattimer & Schramm 1976), or the cataclysmic collapse of a massive star in a very energetic supernova-like explosion (McFayden, Woosley & Heger 1999; Paczyński 1998). The formation of a black hole with a debris torus around it is a common ingredient of both these scenarios. The binding energy of the orbiting debris and the spin energy of the black hole are the two main reservoirs available, the extractable energy being up to  $10^{54}$  ergs (Rees 1999).

A key issue that has remained largely unexplained is what determines the characteristic durations of the bursts (typically between  $10^{-2}$  and  $10^3$  seconds). While bursts lasting hundredths of a second could be derived from a very short, impulsive energy input, this is generally unable to account for the complicated temporal structure found in a

large fraction of the  $\gamma$ -ray burst light-curves (Sari & Piran 1997; Fenimore et al. 1999; Ramirez-Ruiz & Fenimore 1999). This is suggestive of a central engine that releases energy, in the form of a wind or multiple shells, over a period of time commensurate with the observed duration of a GRB (Rees & Mészáros 1994).

The lack of apparent photon-photon attenuation of high energy photons implies substantial bulk relativistic motion. The relativistic shells must have a Lorentz factor,  $\Gamma = (1 - \beta^2)^{-1/2}$ , of the order of  $10^2 - 10^3$  (note that even if – as is likely – the outflow is beamed the spherical shell model is applicable provided the beam is wider than an angle  $\sim \Gamma^{-1}$ ). The observed afterglow emission in this scenario is produced when the expanding shells slow down as a result of the interaction with the surrounding medium.

This internal-external fireball model (Mészáros & Rees 1997; Sari & Piran 1997) requires a complicated central engine which persists (though unsteadily) for much longer than the typical dynamical time scale of a stellar mass compact object, which is of the order of milliseconds.

Observationally, there is a bimodal distribution of burst durations (Kouveliotou et al. 1993). It is a plausible conjecture that the short ( $\lesssim 1$  s) bursts are triggered by coalescing compact binaries, and the long ones by a special kind of supernova-like explosion (we note, furthermore, that those with detected afterglows are all in the long category; this is a selection effect caused by the fact that BeppoSAX has a  $\sim 5$  second trigger).

In the internal shocks scenario for GRBs, the actual burst temporal profile is the outcome of the complex dynamics of the ejecta, which have usually been treated as con-

centric shells moving at different speeds. Although a range of Lorentz factors seems likely, it is not obvious whether most of the energy (or the mass) would be concentrated towards the high or low end of the  $\Gamma$  distribution. In this early phase, the time-scale of the burst and its overall structure follows, to a large extent, the temporal behaviour of the source (Kobayashi, Piran & Sari 1997). In contrast, the subsequent afterglow emerges from the shocked regions of the external medium where the relativistic flow is slowed down; therefore the inner engine cannot be seen directly in the afterglow. The external medium may be typical interstellar matter (ISM;  $\rho_{\text{ext}} \sim 1 \text{ cm}^{-3}$ ), but it would be much denser if a massive star underwent rapid mass-loss before the burst was triggered ( $\rho_{\text{ext}} \gtrsim 10^4 \text{ cm}^{-3}$ , see Ramirez-Ruiz et al. 2001). It is thus of great importance to obtain as much information as possible on the nature of the early relativistic outflow, as this would provide us with some of the best clues to the nature of GRB progenitors.

Long GRBs, which are very complicated in the time domain, may also show multiple episodes of emission, separated by background intervals or quiescent times of variable duration. In earlier discussions (Fenimore & Ramirez-Ruiz 2000, Ramirez-Ruiz & Merloni 2001, hereafter Paper I), the presence of quiescent times has been regarded as an indication of a turning-off of the central site for a period of time. However, if gamma-ray bursts are produced by internal shocks in relativistic winds, it is possible as an alternative to attribute the quiescent times in the  $\gamma$ -ray light-curves to a complicated modulation of the ejecta velocities in the relativistic outflow.

In this paper we explore the feasibility of different internal-external shock models to produce episodes of quiescence in a  $\gamma$ -ray burst. We calculate the expected light-curves of the early multi-wavelength emission. We show that light-curves of the prompt afterglow in the optical, X-ray and  $\gamma$ -ray bands could provide us with strong evidence as to whether or not the central engine goes dormant for a period of time comparable to the duration of the gap.

## 2 QUIESCENT TIMES IN INTERNAL SHOCKS

### 2.1 Model outline

We simulate GRB light-curves by adding pulses radiated in a series of internal shocks that occur in a transient, unsteady relativistic wind. Several authors have modelled this process by randomly selecting the initial conditions at the central site (Daigle & Mochkovich 1998; Kobayashi, Piran & Sari 1997; Spada, Panaitescu & Mészáros 2000). Here we model the wind dynamics and the emission processes as in Fenimore & Ramirez-Ruiz (2000), but we include the effect of the photon diffusion through the colliding shells and the wind on the pulse duration (Spada, Panaitescu & Mészáros 2000).

As described in Fenimore & Ramirez-Ruiz (2000), the wind is discretized in a sequence of  $N$  shells that are ejected over a period  $T_{\text{dur}}$  from the central source, with a range of initial thicknesses ( $\Delta_i$ ). We randomly select  $t_{0i+1} - t_{0i}$  from a Poisson distribution based on the rate of peak occurrence. Thus, we specify the rate of explosions at the central site

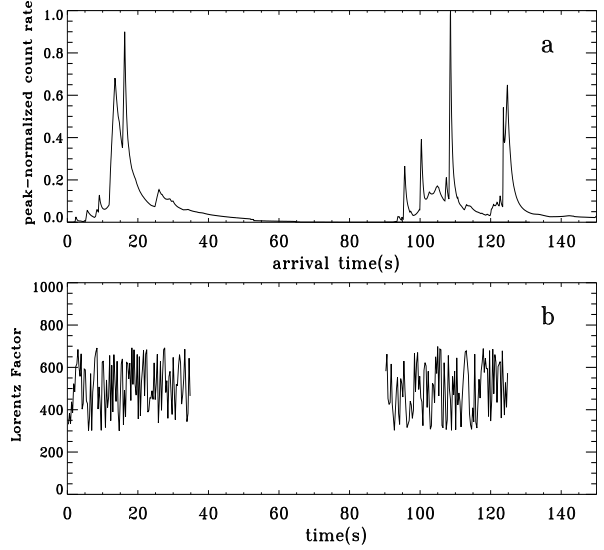


**Figure 1.** Simulations of the effects of turning off the central source in an internal shock model. Panel (a) shows the light-curve at the detector generated by a central engine which emits shells at the mean rate of 1.4 per second, with Lorentz factors chosen randomly between  $3 \times 10^2$  and  $9 \times 10^2$ , and turns off between  $t = 35 \text{ s}$  and  $t = 90 \text{ s}$ , as shown in panel (b) ( $T_{\text{dur}}=125 \text{ s}$ ). The external density has been fixed to  $1 \text{ cm}^{-3}$ .

( $\frac{N}{T_{\text{dur}}}$ ) in such a way that the actual number of peaks is random. We generate about 1.4 shells per second\*. We set the maximum thickness to be  $\Delta_i \sim 0.3 \text{ lt-s}$ . The peak energy can be estimated from the bursts with measured redshifts. GRB970508 had a peak luminosity  $L \sim 3 \times 10^{51} \text{ erg s}^{-1}$ . Other GRBs have been found at extreme redshifts (Kulkarni et al. 1999), implying  $L \sim 2 \times 10^{53} \text{ erg s}^{-1}$ . In our simulations the shell peak energy (isotropic equivalent)  $E_i/4\pi$  is drawn from a log-normal distribution with an average value  $\bar{E} = 10^{51} \text{ erg s}^{-1}$  and a dispersion  $\sigma_E = 10^{1.5} \text{ erg s}^{-1}$ , thus allowing the occasional ejection of very energetic shells.

We calculate the radii where shells collide and determine the emission features for each pulse. If some inner shell moves faster than an outer one ( $\Gamma_i > \Gamma_j$ ), it will overtake the slower one at a radius  $R_i(t_{ij}) = R_j(t_{ij}) = R_c$ . The resulting pulse reaches the detector at the relative time of arrival,

$$T_{\text{toa}} = t_{ij} - \frac{R_c}{c} = t_{0i} + \frac{\Gamma_j^2}{\Gamma_i^2 - \Gamma_j^2} \Delta t_{0ij}, \quad (1)$$

where  $\Delta t_{0ij} = t_{0i} - t_{0j}$  is the difference between the times at which the inner engine generates the  $i$ -th ( $t_{0i}$ ) and the  $j$ -th shell ( $t_{0j}$ ). The collision radius,  $R_c$ , is roughly

$$R_c \sim c\Gamma^2\Delta T, \quad (2)$$

where  $\Delta T$  is the typical time variation observed in a GRB (Rees & Mészáros 1994). For typical values such as  $\Delta T = 0.1$

\* The substantial overlap of the temporal structures in the burst have made the study of individual pulses somewhat difficult. An excellent analysis has been provided by Norris et al. (1996), who examined the temporal structure of bright GRBs by fitting time histories with pulses. They found that the distribution of intervals between pulses exhibits a broad maximum near 0.8 s.

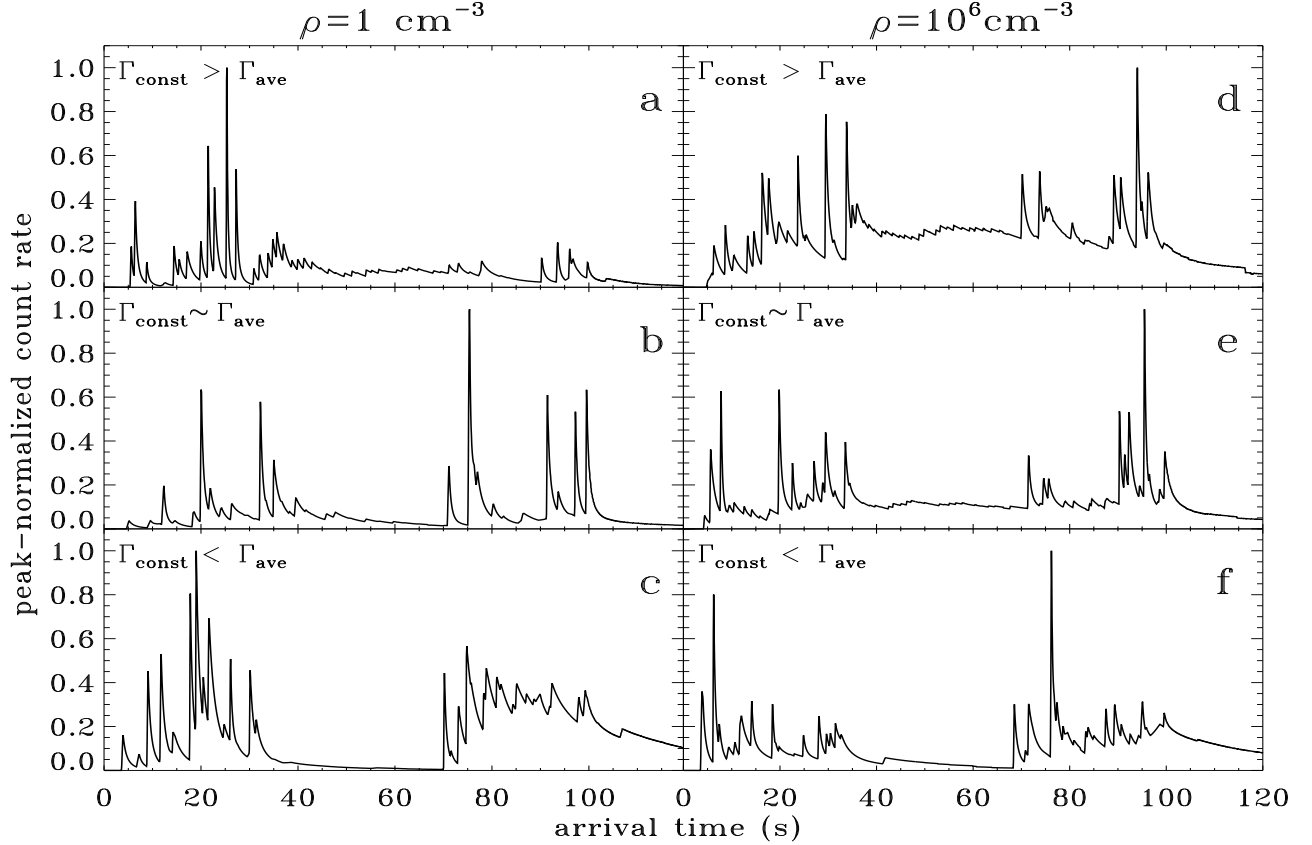


**Figure 2.** Consequences of different steady state scenarios observed in the  $\gamma$ -ray profiles for a burst triggered in two different density environments. The central engine ejects shells with a constant Lorentz factor,  $\Gamma_{\text{const}}$ , between  $t = \frac{1}{3}T_{\text{dur}}$  and  $t = \frac{2}{3}T_{\text{dur}}$  ( $T_{\text{dur}} = 100$  s). The rest of the time the Lorentz factors are randomly selected between  $10^2$  and  $10^3$ . The calculated light-curves for the cases  $\Gamma_{\text{const}} > \Gamma_{\text{ave}} = 550$  (a and d),  $\Gamma_{\text{const}} \sim \Gamma_{\text{ave}}$  (b and e), and  $\Gamma_{\text{const}} < \Gamma_{\text{ave}}$  (c and f) are shown for  $\rho_0=1$  and  $\rho_0=10^6$  respectively. A quiescent time could be observed when the Lorentz factor of the steady flow is much smaller than the average Lorentz factor. The level of the underlying smooth component produced by collisions with the steady ejecta increases as the product  $\rho_0\Gamma_{\text{const}}^2$  is increased.

to 1.0 s,  $R_c$  is about  $10^{14}$  cm. As the fast later shells move outward they begin to interact with the external medium and decelerate. The deceleration is expected to occur at

$$R_{\text{dec}} = 10^{16.7} \left( \frac{E_{52}}{\rho_0 \theta^2} \right)^{1/3} \Gamma_2^{-2/3} \text{ cm}, \quad (3)$$

where  $E_0 = 10^{52} E_{52}$  ergs is the initial fireball energy,  $\Gamma_0 = 10^2 \Gamma_2$  is the terminal coasting bulk Lorentz factor and  $\rho = 1\rho_0 \text{ cm}^{-3}$  is the average external density.

The radius of deceleration depends on the product  $\rho_0\Gamma_0^2$ , so that large variations of  $\rho_0$  can be mimicked by much smaller variations in  $\Gamma$ . We should remark that the ejecta Lorentz factors are limited to  $\Gamma > 30$  (Mészáros, Laguna & Rees 1993), and are unlikely to exceed by much the value  $\Gamma \sim 10^3$  (Ramirez-Ruiz & Fenimore 2000). The value of  $R_{\text{dec}}$  is crucial in determining whether (and at which distance) the slower inner shells will eventually catch up with the outer ones as they are decelerated (Fenimore & Ramirez-Ruiz 2000).

For each collision between two shells there is a reverse and a forward shock. The shock jump equations determine the physical parameters of the shocked fluids, the velocity of the shock fronts and the thickness  $\Delta_{ij}$  of the merged

shell at the end of the collision. We assume that in between two consecutive collisions the thickness of the shell increases proportionally to the fractional increase of its radius  $\frac{d\Delta_i}{\Delta_i} \propto \frac{dR}{R}$  (Spada, Panaitescu & Mészáros 2000). The ejection parameters determine the dynamics of the wind and the pulse dynamical efficiency,  $\epsilon_{ij}$ . This efficiency reflects the differences between the Lorentz factors of a pair of colliding shells ( $\Gamma_i > \Gamma_j$ ). The efficiency for an individual collision can be calculated from the initial and final bulk energies,

$$\epsilon_{ij} = 1 - \frac{m_{ij}\Gamma_{ij}}{m_i\Gamma_i + m_j\Gamma_j} \quad (4)$$

where  $\Gamma_{ij}$  is the Lorentz factor of the resulting shell:

$$\Gamma_{ij}^2 = \Gamma_i\Gamma_j \frac{m_i\Gamma_i + m_j\Gamma_j}{m_i\Gamma_j + m_j\Gamma_i}, \quad (5)$$

and the resulting mass is  $m_{ij} = m_i + m_j$ .

The first collisions remove the initial random differences between the Lorentz factors of successive shells. If the mean Lorentz factor  $\bar{\Gamma}$  remains steady for the entire burst duration, then the efficiency steadily decreases during the wind expansion. If  $\bar{\Gamma}$  is modulated on a timescale much smaller than the overall duration of the wind, dynamically efficient

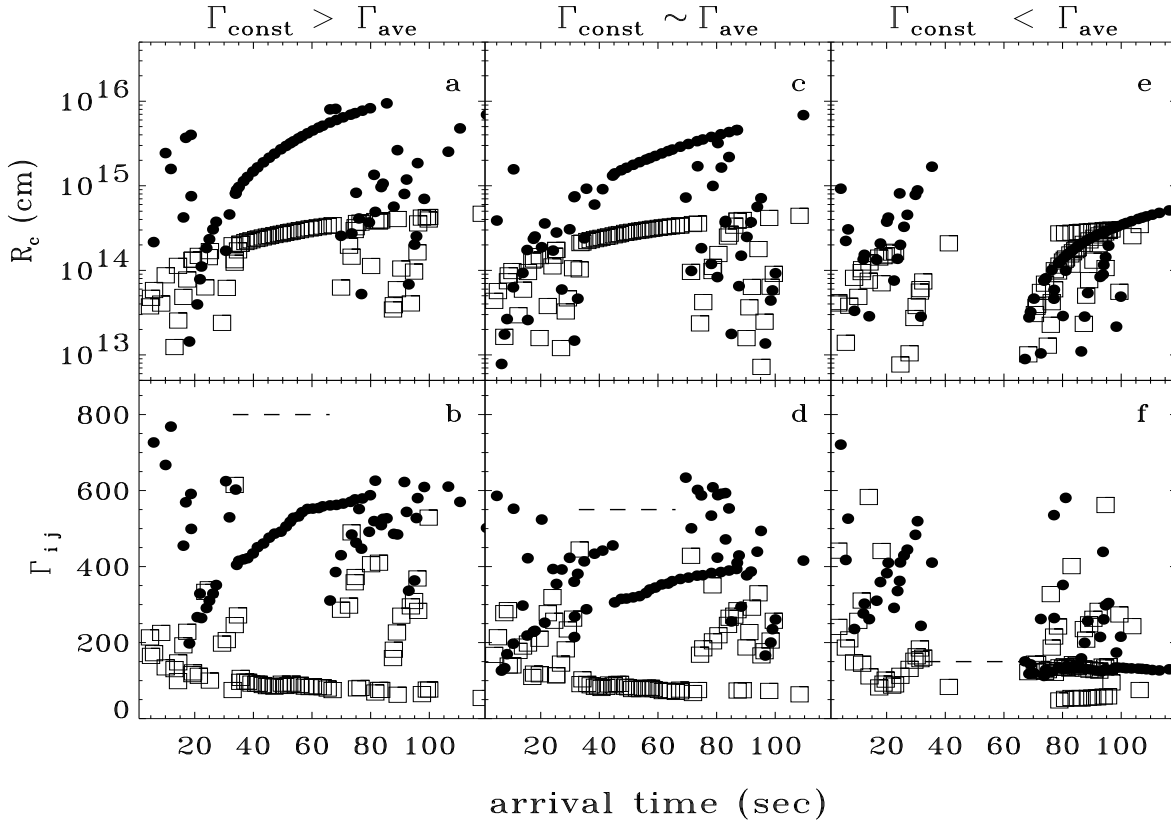


**Figure 3.** Collisional parameters of the internal shocks produced in the simulations of three steady outflow cases (see text for more details) corresponding to the light-curves shown in Fig. 2. Filled circles correspond to the low density case ( $\rho_0 = 1$ ) and open squares to the high density case ( $\rho_0 = 10^6$ ). Plotted are the radii  $R_c$  where the collisions take place and the resulting Lorentz factors  $\Gamma_{ij}$  as functions of the relative times of arrival at the detector,  $T_{toa}$ . The radii of collision for a central engine that ejects, during its steady state, faster shells ( $\Gamma_{const} > \Gamma_{ave} = 550$ ), average speed shells ( $\Gamma_{const} \sim \Gamma_{ave}$ ), and slower shells ( $\Gamma_{const} < \Gamma_{ave}$ ), are shown in panels (a), (c) and (e) respectively. The resulting Lorentz factors as functions of arrival time for each of these scenarios are shown in panels (b), (d) and (f), respectively. The dashed lines in panels (b), (d) and (f) mark the value of  $\Gamma_{const}$  in the three cases.

collisions at large radii are still possible. In most earlier discussions (see e. g. Kobayashi, Piran & Sari 1997), the concern was raised that internal shocks without deceleration were rather inefficient, converting only  $\lesssim 25\%$  of the bulk motion energy into radiation. Since the afterglows can only account for a few percent of the radiated energy, it was unclear where most of the energy goes. However, Fenimore & Ramirez-Ruiz (2000) showed that, for large values of  $\Gamma$  (or large values of the ambient density), deceleration is an effective catalyst for converting the bulk motion energy into radiation.

## 2.2 Turning off the central engine: a discontinuous wind

To simulate the effects of a complete turn-off of the central site, we impose a quiet emission time in the activity of the engine (i.e. the source does not emit any shells) for about 55 seconds. Before and after this interval, shells are generated at the mean rate of about 1.4 per second, with the shell Lorentz factors  $\Gamma_i$  randomly selected between  $\Gamma_{min}$  ( $3 \times 10^2$ ) and  $\Gamma_{max}$  ( $9 \times 10^2$ , see Fig. 1b).

As the time of arrival of the pulses at the detector

closely reflects the activity at the central engine (Kobayashi, Piran & Sari 1997), it is not surprising that we find a quiescent time in the  $\gamma$ -ray light-curve (see Fig. 1a), with a duration comparable to the quiet emission period at the central engine. This is generally the case whenever the central engine turns off for a long enough time and the internal shocks develop well inside the radius where the external shock decelerates (Fenimore & Ramirez-Ruiz 2000).

The presence of a quiet emission period in the central engine would divide the relativistic outflow into two well separated thick shells, each of them composed of many concentric inner shells moving at different (relativistic) speeds. In section 3 we will discuss in detail the clear signatures observable in the afterglow emission when the relativistic flow is discontinuous.

## 2.3 Modulating a continuous relativistic wind

There are at least two simple mechanisms which might lead to a period of quiescent emission in the observed light curve without postulating any quiet phase in the central engine. The simplest possibility is that the central engine ejects consecutive shells moving with Lorentz factors that are es-

essentially constant over a certain period of time,  $\Delta t_{\Gamma=\text{const}}$ . In this scenario (which will be referred to in the following as steady outflow) the requirement is that the difference in Lorentz factors of two consecutive shells  $\Gamma_i, \Gamma_j$ , ( $i > j$ ) be small enough ( $\Gamma_i - \Gamma_j < \epsilon$ ) for the shells not to collide until the deceleration radius (see Eq. 3). The second possibility may arise when the Lorentz factors of a series of consecutive shells monotonically decrease ( $\Gamma_i < \Gamma_j$ ) during a certain time interval  $\Delta t_{\partial\Gamma < 0}$ . In both cases, an observed quiescent time interval will be a consequence of the modulation of a continuous wind.

### 2.3.1 Steady outflows in relativistic ejecta

To simulate the effects of a steady outflow, we impose a period  $\Delta t_{\Gamma=\text{const}}$  of constant velocity of the ejecta, in between two intervals during which the shells' Lorentz factors  $\Gamma_i$  are randomly selected between  $\Gamma_{\min}$  ( $10^2$ ) and  $\Gamma_{\max}$  ( $10^3$ ). The value of the shells' Lorentz factor in the steady state phase,  $\Gamma_{\text{const}}$ , is also chosen to lie between  $\Gamma_{\min}$  and  $\Gamma_{\max}$ . The properties of the observed light-curve will depend crucially on the value of  $\Gamma_{\text{const}}$ . In particular, it is this value that essentially determines if a quiescence period is present or not in the light-curve. We denote as  $\Gamma_{\text{ave}} = (\Gamma_{\min} + \Gamma_{\max})/2$  the average Lorentz factor of the shells randomly emitted before and after the steady state phase.

The light-curves for three different steady states,  $\Gamma_{\text{const}} > \Gamma_{\text{ave}}$ ,  $\Gamma_{\text{const}} \sim \Gamma_{\text{ave}}$  and  $\Gamma_{\text{const}} < \Gamma_{\text{ave}}$  are shown in figures 2a, 2b and 2c, respectively, for the low density case ( $\rho_0 = 1$ ), and in figures 2d, 2e and 2f, respectively, for a very high density case ( $\rho_0 = 10^6$ ).

In the high  $\Gamma_{\text{const}}$  case (Fig. 2a, 2d), the interaction of the steady flow with the early ejected material produces a low intensity component of  $\gamma$ -ray emission. This underlying smooth component decreases in intensity as the Lorentz factor of the steady flow becomes progressively smaller (see Fig. 2b, 2e) and, depending on the background level, could be interpreted as the signature of a quiescent time. When  $\Gamma_{\text{const}}$  is much smaller than the average Lorentz factor of the merged shells (Fig. 2c, 2f), the photon emission takes place later, producing a much clearer quiet interval in the time history. If the central engine ejects relativistic matter with a constant energy rate (so that the slower shells are more heavily loaded with baryons), one would expect the later observed emission to be more energetic due to the super-imposition of the two contributions (see Fig. 2c, 2f).

Clearly the level of the underlying smooth component associated with the steady phase increases with increasing the value of the product  $\rho_0 \Gamma^2$ . Thus, for a fixed range of ejecta Lorentz factors, the presence of quiescent times in  $\gamma$ -ray light-curves is more evident in low density environments.

The exact dynamics of these different scenarios can be more easily understood with the help of Figure 3, which shows the radii  $R_c$  where the collisions between shells take place, together with the resulting Lorentz factors  $\Gamma_{ij}$ , as functions of the time of arrival  $T_{\text{toa}}$  at the detector (see Eq. 1).

At the end of the first ejection phase of shells with random velocities, we are left with a rather ordered flow in which the faster (merged) shells are the outermost ones and the slower ones follow behind. The dynamics of the ejecta are mainly determined by the value of the deceleration radius

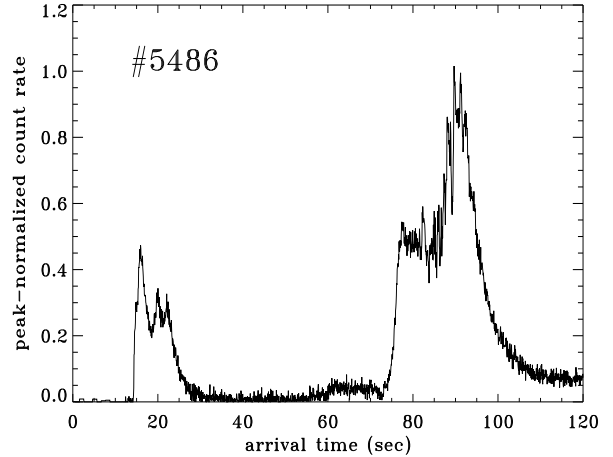


**Figure 4.** The time history of the long BATSE burst #5486. Note the presence of narrow peaks throughout the time history over an underlying smooth emission that seems to be increasing with time. The presence of such quiescent time may arise from a central engine which emits relatively slow shells during its steady phase, as shown in figure 2c.

(Eq. 3), which in turn depends on the external density and on the ejecta Lorentz factors. For a given  $\Gamma_0$ , the denser the external environment the smaller the radius of deceleration,

$$R_{\text{dec}} \sim \begin{cases} 10^{16} \text{ cm} & \text{if } \rho_0 \simeq 1 \\ 10^{14} \text{ cm} & \text{if } \rho_0 \simeq 10^6, \end{cases} \quad (6)$$

(see Eq. 3, where we have assumed  $E_{52} = 1$  and  $\Gamma_2 = 3$ ).

Consequently, if the source is surrounded by a high density medium, a substantial fraction of the internal collisions would take place at  $R_{\text{dec}}$  as the ejecta interact with the rapidly decelerating outer shell. The merged shells produced by these collisions will have relatively low Lorentz factors  $\Gamma_{ij}$ .

If  $\Gamma_{\text{const}} > \Gamma_{\text{ave}}$ , the fast steady outflow will overtake the early emitted ejecta at a large radius (see Fig. 3a), thermalizing their energy and boosting the Lorentz factor of the shell (see Fig. 3b). When the external density is higher, the fast steady outflow will overtake the decelerating shell at a radius  $R_c \gtrsim R_{\text{dec}}$  (see open squares in Fig. 3a). The resulting Lorentz factor in this case will be much lower. The observed time over which internal shocks transform the relative kinetic energy of the two colliding layers is of the order of  $R_c/c\Gamma_{ij}^2$ . Thus, it is the emission from these collisions at large radii (and/or small Lorentz factors) that ‘fills the gap’ in the  $\gamma$ -ray light-curves (see Fig. 2a and 2d) with a number of low intensity, but large width, pulses.

A similar behaviour is seen when the Lorentz factor of the steady state is close to the average value  $\Gamma_{\text{ave}}$ .

Finally, when the source ejects very slow shells ( $\Gamma_{\text{const}} < \Gamma_{\text{ave}}$ ) during the steady state phase, the expected behaviour can lead to two different scenarios.

If the burst is triggered in a low density environment, the later, faster emission will overtake the steady ejecta before they reach the decelerating external shock (see filled circles in Fig. 3e). If instead the burst is triggered in a dense environment, the earlier ejected (faster moving) shells will

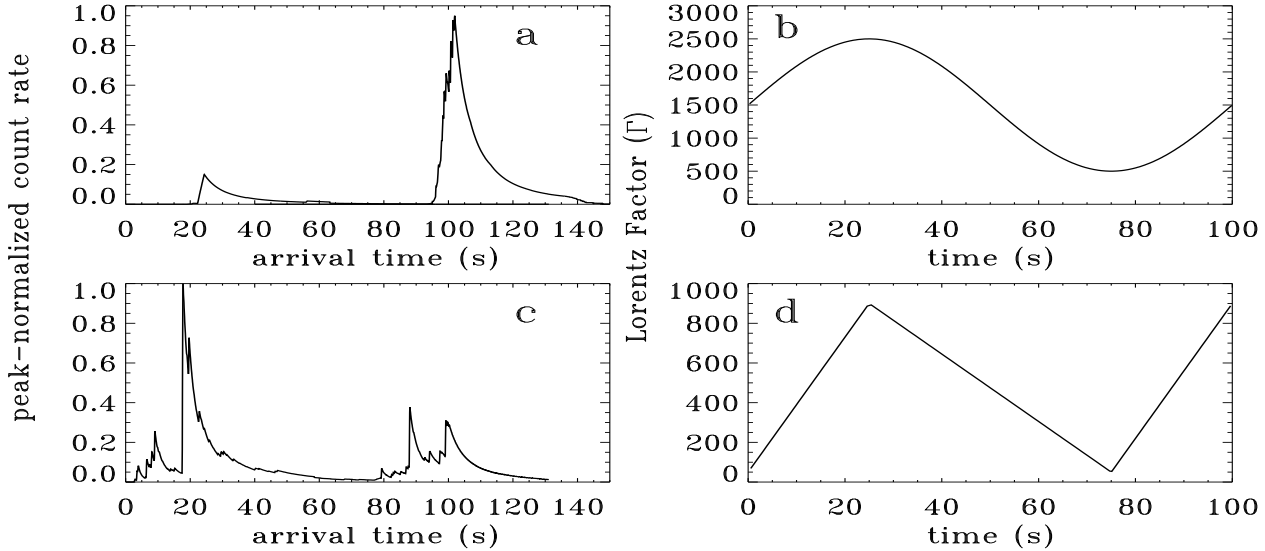


**Figure 5.** Simulations of what happens when the central engine modulates the mean Lorentz factor in an internal shock model ( $\rho_0 = 1$ ). Panel (a) shows the light-curve due to a wind modulated by a sinusoid with period  $P = T_{\text{dur}} = 100$  s, as shown in panel (b). Panel (c) shows the light-curve due to a wind modulated by a triangular function, as shown in panel (d).

begin to interact with the surrounding medium and decelerate before they are caught up by the later shells. Figures 3e and 3f show the collisional parameters  $R_c$  and  $\Gamma_{ij}$  for this scenario in the two cases.

In our example, the values of the ejecta Lorentz factors are such that the later emitted shells overtake the steady ejecta. This causes the photon emission from these collisions to arrive later at the detector, creating a period of quiescence in the GRB light-curve of duration comparable to the duration of the steady state phase of the flow (see Fig. 2c and 2f). Furthermore, the late pulses arriving from these collisions give rise to a higher underlying smooth level after the quiescence period.

Figure 4 shows the BATSE time history of the burst 5486, that has the characteristics foreseen in the latter scenario. It has many narrow peaks throughout its time history and an underlying smooth component that seems to be increased after the second emission episode. However, it is also possible that the apparent increase of the background emission is due to a continuing underlying source.

### 2.3.2 Winds with monotonically decreasing speed

The second possibility for a modulated wind to produce a quiescence period in the observed  $\gamma$ -ray light-curve, is to have in the flow a series of shells with monotonically decreasing Lorentz factors. We use two different functions to model such modulation: a sine function with period  $P = T_{\text{dur}}$  (Fig.

5b), and a triangular one (Fig. 5d), which accounts for a power-law decline of the Lorentz factors. In both cases, the time ( $\Delta t_{\partial\Gamma < 0}$ ) during which consecutive ejected shells have decreasing velocities is equal to  $\frac{T_{\text{dur}}}{2} = 50$  s.

As can be seen in Fig. 5a, the sine modulation is more likely to give rise to a temporal profile that shows precursor activity, while in the case of a triangle modulation (Fig. 5b), the first episode of emission can be more intense.

## 2.4 X-ray emission from internal shocks

The process by which the dissipated energy is finally radiated depends on the energy distribution of protons and electrons in the shocked material and on the values of the comoving density and magnetic field. The internal shocks heat the expanding ejecta, amplifying the preexisting magnetic field or generating a turbulent one, and accelerate electrons, leading to synchrotron emission and inverse Compton scattering. Rees & Mészáros (1994), Papathanassiou & Mészáros (1996) and Sari & Piran (1997) calculated the radiation spectrum assuming that the electrons come into (at least partial) equipartition with the protons. If a fraction  $\varepsilon_e$  of the dissipated energy goes into the electrons, their characteristic Lorentz factor is given by  $\Gamma_e \sim \varepsilon_e \varepsilon_{\text{dis}} / m_e c^2$ , where  $\varepsilon_{\text{dis}}$  is the dissipation efficiency, i.e., the amount of kinetic energy that is converted into internal energy (a more realistic treatment, that considers a power-law distribution for the accelerated electrons can be found in Spada,

Panaitescu & Mészáros 2000). The magnetic field  $B$  is parameterised by the fraction  $\varepsilon_B$  of the energy of the shocked gas that it contains:  $B^2 = 8\pi\varepsilon_B\epsilon_{\text{dis}}n'_e m_p c^2$ , where  $n'_e$  is the comoving frame electron number density of the shocked fluid. Assuming  $L = 10^{52}$  erg s $^{-1}$  and  $\varepsilon_B = 1/3$  (complete equipartition between protons, electrons and the magnetic field), the value of the magnetic field at the radius  $R_c \sim c\Delta T\bar{\Gamma}^2 \simeq 2.7 \times 10^{14} (\Delta T/1 \text{ s})(\bar{\Gamma}/300)^2$  cm, where most of the collisions take place, is  $B_{\text{eq}} \sim 10^3 - 10^4$  G (Daigne & Mochkovich 1998; Papathanassiou & Mészáros 1996), also depending on the ratio  $\Gamma_i/\Gamma_j$  (Eq. 5). Synchrotron emission will occur at a typical energy,  $h\nu_{\text{syn}}$  (in the observer frame);  $\gamma$ -rays can be produced by inverse Compton scattering of the synchrotron photons on the accelerated electrons at a typical energy (Daigne & Mochkovich 1998)

$$h\nu_{\text{IC}} \simeq h\nu_{\text{syn}}\Gamma_e^2 \sim 500 \left(\frac{\Gamma_{ij}}{300}\right) \left(\frac{B_{\text{eq}}}{1000 \text{ G}}\right) \left(\frac{\Gamma_e}{100}\right)^4 \text{ keV}. \quad (7)$$

The spectrum of the overall burst is the sum of all the contributions from the individual collisions in the internal shock scenario. The typical radiation energy of each pulse then depends on the resulting Lorentz factor,  $\Gamma_{ij}$ . Thus, it is possible that the presence of a quiescent time in the  $\gamma$ -ray light-curve is due to the shifting of the internal shock emission into longer wavelength bands. This will happen when the value of the resulting Lorentz factor (for a fixed luminosity) is sufficiently small or when the luminosity drops substantially for a certain period of time (given a constant mass loss rate). However, when the optical thickness of the emitting shells is greater than unity, the photons are down-scattered by the cold electrons before they escape, leading to a further decrease in their energy. The optical thickness in turn is determined by the wind luminosity  $L$ , the range of Lorentz factors of the wind (which determines the collision radii), and the density of the external medium.

Indeed, in the case of a very high density environment, the underlying smooth component shown in Fig. 2 and discussed in section 2.3.1, will tend to be softer than the overall burst emission. Depending on the exact values of the magnetic field and the dynamical parameters, this underlying feature may disappear from the  $\gamma$ -ray emission and appear as hard X-ray radiation. For example, from the simulation described in Figure 3c and 3d (open squares), assuming  $B \sim 10^3$  G and  $\Gamma_e = 100$ , the energy of the resulting pulses responsible for the underlying smooth component (with Lorentz factors,  $\Gamma_{ij} \sim 25 - 50$ ), will be  $h\nu_{\text{IC}} \simeq 30 - 70$  keV. Figure 6 shows the BATSE time history of the burst 6576 which may be consistent with the above scenario, in that there is a period of quiet emission only in the high energy channel. An inspection of the high energy channel alone might have led one to postulate the presence of a quiet time in the central engine activity, but even a cursory examination of the low energy channel reveals that this is not the case (note that BATSE high resolution light-curves are obtained in the 25 – 1000 keV range). Alternatively, in the low density environment and for the  $\Gamma_{\text{const}} < \Gamma_{\text{ave}}$  case (see filled circles in Fig. 3e and 3f), the emission episode following the quiescent time will be much softer than the preceding one.

Observations of the prompt X-ray emission in GRBs exhibiting quiescent times in their light-curves can be used to constrain the inner engine emission properties. Any qui-

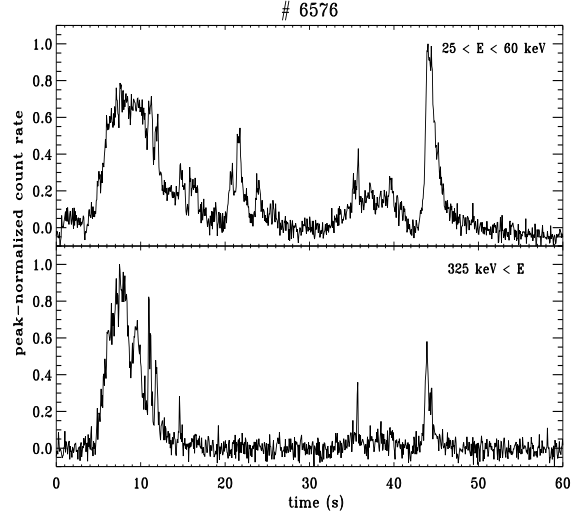


**Figure 6.** The time history of the long BATSE burst #6576. Note the presence of a quiescent interval that is near background in the highest energy channel but that is absent in the low energy one. Thus a measurement in a single energy channel is inadequate for the correct identification of a complete turn-off of the central engine. Additionally, due to the limited spectral range of BATSE a non-detection in all four energy channels does not necessarily indicate a complete absence of central engine activity.

escent time detected simultaneously in the X-ray and  $\gamma$ -ray bands will imply that, for a comparable time, the central source has either completely switched off or entered a steady state phase characterised by a very small luminosity (and/or very small Lorentz factor  $\Gamma_{\text{const}}$ ). As an example, we mention GRB 990510, detected by BeppoSAX and BATSE (Kuulkers et al. 2000), that shows no sign of emission between 40 and 700 keV for a period of about 30 seconds.

## 2.5 Continuous vs discontinuous

The main conclusion we can draw from the simulations presented above is that, in the framework of the internal shocks model, there are realistic assumptions that produce a long quiescent interval in a GRB light-curve, without having to postulate that the central source itself turns off for a comparably long time.

Of course, as shown in Fig. 1a, a quiet emission event is *always* observed if the central engine turns off for a long enough time (provided that little deceleration is occurring, see Fenimore & Ramirez-Ruiz 2000), and the duration of the observed period of quiescence in the  $\gamma$ -ray light-curve would correspond to the duration of the quiescence time in the central source.

On the other hand, for the wind modulations we have discussed, this is not always the case. For the steady state modulation, as already pointed out, the actual duration of the observed quiescent time will depend on the Lorentz factor of the steady flow. In the most favourable case ( $\Gamma_{\text{const}} < \Gamma_{\text{ave}}$ , Fig. 2c), we have simulated  $10^3$  bursts, with a fixed  $\Delta t_{\Gamma=\text{const}}$ , and found that the average quiescent time in the light-curve is shorter than  $\Delta t_{\Gamma=\text{const}}$  by a factor of about 1.3. For the sinusoidal and triangular modulations, again we simulated  $10^3$  temporal profiles for each of the two cases, keeping fixed  $\Delta t_{\partial\Gamma < 0}$ . The resulting quiescent times in the

$\gamma$ -ray light-curve are on average shorter than  $\Delta t_{\partial\Gamma < 0}$  by almost a factor of 2. This means that, in order to produce an observed quiescent period of, for example, 30 seconds, the source has to emit a series of shells with decreasing Lorentz factors for about a minute. This poses severe constraints on any dynamical model for the inner engine.

How, in the light of our internal shocks simulations, is it possible to discriminate between the different scenarios, and in particular, to determine if the central source really turns off in correspondence to an observed quiescent time?

As we have seen, each of the cases described above has its own characteristic features; however, these are not always unique. For example, the sine modulation is more likely to give rise to a temporal profile that shows precursor activity (see Fig. 5a), while the ‘steady phase’ modulation can produce almost any observed quiescent time profile, as a consequence of the complex dynamics of the relativistic ejecta. This is mainly due to the large amount of free parameters that the internal shock model offers to describe the great variety of GRBs.

However, if the central source really turns off for a long period when a quiescent time is observed in the  $\gamma$ -ray and X-ray light-curves, the relativistic flow will be discretised in a number of thick shells, each one of size roughly comparable to the duration of the different emission episodes observed at the detector. This will not be the case if such features arise from the modulation of the relativistic ejecta, because all these scenarios envisage the ejection of a continuous outflow over the whole duration of the main event at the central engine.

For this reason it is of the utmost importance to obtain as much information as possible on the nature of the relativistic flow, as this would provide us with some of the best clues on the stability properties of the GRB engine (see Paper I). Thus, in the following sections, we study the expected prompt (early afterglow) multi-wavelength signal. We show that this early signal could help us determine whether or not a gap in the  $\gamma$ -ray light-curve was caused by a turn-off of the central engine as opposed to a modulation of the relativistic wind.

### 3 THE EARLY AFTERGLOW

The internal shocks we discussed in the previous section are produced by the collisions of different components of the relativistic outflow travelling at different velocities. When the ejecta run into the external medium two more shocks are produced: a short-lived reverse shock, traveling through the ejecta; and a long-lived forward shock propagating in the swept-up ambient material. In the following sections we describe the expected emission from the two external shocks (forward and reverse), focusing in particular on the distinctive signature to be expected from GRBs exhibiting a quiescent time in their light-curves.

#### 3.1 The forward shock

The synchrotron spectrum from relativistic electrons that are continuously accelerated into a power law energy distribution comprises four power-law segments, separated by three critical frequencies: the self absorption frequency ( $\nu_{\text{sa}}$ )

the cooling frequency ( $\nu_c$ ) and the characteristic synchrotron frequency ( $\nu_m$ ) (Sari, Piran & Narayan 1998; Mészáros, Rees & Wijers 1998). The spectrum and the light-curve of an afterglow are determined by the time evolution of these frequencies, which in turn depends on the hydrodynamical evolution of the fireball. The main temporal and spectral features of the expected afterglows have been discussed in Mészáros, Rees & Wijers (1998); Sari & Piran (1999).

Here, we explore the hydrodynamics of the relativistic fireball expanding in a uniform external medium, and the evolution of the bolometric luminosity, without considering any spectral characteristic. The treatment in this section is approximate and correction factors may need to be included in a more precise treatment.

The interaction of the outer shell with the external medium is described by the adiabatic Blandford-McKee (1976) self-similar solution. In the early afterglow, as the shell progressively collects material from the external medium, the Lorentz factor initially stays constant. Due to the increase in the area of the shell, the internal energy increases with time as  $\sim t^2$ . Assuming that the cooling is fast, the observed luminosity is proportional to the internal energy, and so  $L \sim t^2$ .

After this phase, the evolution can be of two types (Sari 1997), depending on the thickness of the wind shell, on its average Lorentz factor and on the external density; shells satisfying  $\Delta > (E_0/\rho_0 m_p c^2)^{1/3} \Gamma_0^{2/3}$  are considered thick, otherwise they can be regarded as thin (Sari & Piran 1999) (here  $E_0$  is the energy of the wind shell sweeping up the external density).

Thick shells, which are usually associated with long bursts, start a decelerating phase, with  $\Gamma(t) \sim t^{-1/4}$ , after a time (Sari 1997)

$$t_N \sim \left( \frac{E_0}{\Delta \rho_0 m_p c^4 \Gamma_0^8} \right)^{1/2}, \quad (8)$$

where  $\Delta$  is the thickness of the wind shell. During this phase, the luminosity is constant and its value is about  $L \sim cE_0/2\Delta$ . This behaviour will continue until the shell has given the surrounding material an energy comparable to its initial energy, then a transition to a faster deceleration phase follows, with  $\Gamma(t) \sim t^{-3/8}$ . This second transition occurs at a time

$$t_{\text{dec}} \sim \left( \frac{E_0}{\rho_0 m_p c^5 \Gamma_0^8} \right)^{1/3}. \quad (9)$$

In this late phase the observed luminosity decreases with time as  $L \propto t^{-1}$ .

Thus, in the case of long bursts (thick wind shells), the signals from the internal shocks and from the early forward shock afterglow overlap, since most of the energy is extracted during a time of duration  $\Delta/c$ . It is worth noting that for thin shells, which usually correspond to short bursts, there is no intermediate stage of constant luminosity (Sari 1997).

If the main  $\gamma$ -ray burst is produced by internal shocks, then the width of the wind shell can be inferred directly from the observed main burst duration:  $\Delta = cT_{\text{dur}}$ . However, if the central engine turns off for a certain period of time, the relativistic outflow will be discretised, causing the width of the wind shell responsible for sweeping up the external medium to be smaller. Thus, apart from the differences in



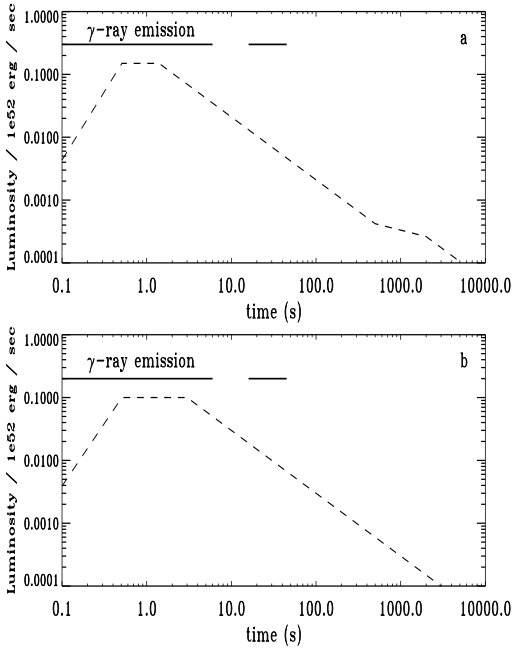


**Figure 7.** Bolometric luminosity of the shocked ISM ( $\rho_0 = 1$ ; dashed line) as a function of time for two different mechanisms of gap production in a  $\gamma$ -ray light-curve (solid line). The case of a central engine that turns off is shown in the upper panel (a), while the case of a modulated continuous wind is shown in the lower one (b). At early stages the Lorentz factor is constant, and the luminosity increases due to the increase of shell area. When the shell has given the ISM an energy comparable to its initial energy, a self-similar solution is established. In this phase the luminosity drops as  $t^{-1}$ . An intermediate state,  $t^{-1/4}$ , may occur for thick shells, leading to constant luminosity. Both cases use  $E_{\text{tot}} = 10^{53}$  ergs,  $\Gamma_0 = 500$  and the internal Lorentz factor within the flow are chosen as in Fig. 1 (for the case (b)  $\Gamma_{\text{const}} = 200$ ).

the main burst properties already discussed in section 2 (c.f. Fig. 1 and 2), one can expect a difference in the relevant transition times of the forward shock evolution (Eqs. 8 and 9).

Figure 7 illustrates the two different afterglow behaviours we expect for a GRB exhibiting a quiescent time of ten seconds between  $t = 6$  s and  $t = 16$  s. We have fixed  $\Gamma_0 = 500$  and the internal Lorentz factors within the flow are chosen as in Figure 1. The external density has been chosen to be the typical ISM one ( $\rho_0 = 1$ ). In the first case (Fig. 7a), the observed period of quiescence is produced by a central engine that turns off (as discussed in section 2.2); in this scenario, the relativistic outflow is divided into two well separated thick shells, an outer and an inner one, of thickness  $\Delta_{\text{out}} = 1.8 \times 10^{11}$  cm and  $\Delta_{\text{in}} = 8.7 \times 10^{11}$  cm, respectively. In the alternative scenario (Fig. 7b), the observed quiescent time is due to a steady state modulation of a continuous relativistic wind (as discussed in section 2.3.1), composed of a single shell of thickness  $\Delta = cT_{\text{dur}} = 1.35 \times 10^{12}$  cm. In both cases we have fixed  $E_{\text{tot}} = 10^{53}$  ergs, but this energy is shared differently by the different shells sweeping up the external medium: in the continuous wind case we have

$E_0 = E_{\text{tot}}$ , while in the discontinuous one the energy of the outer shell is  $E_{0,\text{out}} = E_{\text{tot}} \Delta_{\text{out}} / (\Delta_{\text{out}} + \Delta_{\text{in}}) = 0.17 E_{\text{tot}}$ . The difference in the thickness of the outer shell (the one that interacts with the surrounding medium) is responsible for the dissimilarity in duration of the constant luminosity phase of the afterglow light-curve.

When a quiescent time in the main  $\gamma$ -ray emission is observed after a very short pulse, the difference  $t_{\text{dec}} - t_N$  in the two cases may be large enough to allow us to establish whether the central engine has turned off or not by looking at the detail of the long wavelength afterglow emission. However, if the quiescent time appears after a long period of emission, such discrimination may be very difficult.

We would also like to emphasise that if the burst is located in a denser environment ( $\rho_0 \gtrsim 10^4$ ), expected if the source is associated with the collapse of a massive star, the hydrodynamical evolution would take place on smaller timescales (see Eqs. 8 and 9) and the bolometric luminosity will start declining after a few hundredths of a second.

Furthermore, in the case in which the central engine turns off to produce the observed quiescent time, one expects a collision between the outer shell (which, after the internal shocks have taken place is left with an energy  $E_{\text{out}}$ ) and the inner one (with energy  $E_{\text{in}}$ ). The overall effect of the collision will be, at a fixed frequency, the increase of the flux by a factor of  $\sim (1 + E_{\text{in}}/E_{\text{out}})^{1.4}$  (Kumar & Piran 2000) after about  $10^3$  seconds, as shown in Figure 7a. Once more, if the external medium is much denser, this bump in the light-curve would be observed earlier, as the collision will take place closer in, its exact location depending on the external density and on the dynamical parameters of the two shells (Kumar & Piran 2000).

From Figure 7 it is also clear that the signals from the internal shocks (the main GRB, see Fig. 8 for the light-curve) and the early forward shock emission overlap. Therefore, it might be difficult to detect the smooth external shock component and probably even more difficult to discriminate between the two scenarios by looking for any increasing underlying background component in the  $\gamma$ -ray light-curve (as discussed in section 2.3.1 and in Fig. 4).

In the next section we will show that the early detection of the prompt emission from the reverse shock could in principle be a much clearer test that would help us to discriminate between the two alternative scenarios.

### 3.2 The reverse shock

The reverse shock gives the right magnitude for the observed prompt optical flash with reasonable energy requirements of no more than a few  $10^{53}$  ergs emitted isotropically (Mészáros & Rees 1997). The ejecta cool adiabatically after the reverse shock has passed through and settle down into a part of the Blandford-McKee solution that determines the late profile of the shell and the external medium. Thus, unlike the continuous forward shock emission, the reverse shock terminates once the shock has crossed the shell and the cooling frequency has dropped below the observed range. The reverse shock contains, at the time it crosses the shell, an amount of energy comparable to that in the forward one. However, its effective temperature is significantly lower (typically by a factor of  $\Gamma$ ). Using the shock jump condition and assuming the electrons and the magnetic field acquire a fraction

$\varepsilon_e$  and  $\varepsilon_B$ , respectively, of the equipartition energy, one can describe the hydrodynamic and magnetic conditions behind the shock. For the reverse shock, the two frequencies that determine the spectrum, the cooling ( $\nu_c$ ) and the synchrotron ( $\nu_m$ ) one, are easily calculated by comparing them to those of the forward shock (Mészáros & Rees 1997; Mészáros & Rees 1999; Sari & Piran 1999). Assuming that the forward shock and the reverse shock move with a similar Lorentz factor, the reverse shock frequency at the peak time,  $t_p$ , is given by

$$\nu_p \simeq 2.1 \times 10^{14} \left( \frac{\varepsilon_e \Gamma_0}{30} \right)^2 \left( \frac{\varepsilon_B}{0.3} \right)^{1/2} \rho_0^{1/2} \text{Hz}, \quad (10)$$

which, in the low density case, favours strong optical emission (Sari & Piran 1999). The peak time can be estimated with the help of  $t_p = \max[t_{\text{dec}}, \Delta/c]$ . After this time self-similar evolution begins. Under the flux-freezing field behaviour, for an adiabatic case ( $\Gamma \propto r^{-3/2}$ ) and an electron index  $p = 2$ , the photon spectral index above  $\nu_m$  is  $\beta = -1/2$  ( $F_\nu \propto \nu^\beta$ ). The spectral flux,  $F_\nu$ , has an approximate time dependence of  $t^{-2.1}$  (see Mészáros & Rees 1999 for different spectral behaviours), which is in rough agreement with the ROTSE observations of GRB990123 (Akerlof et al. 1999 report a  $t^{-2}$  dependence for about 600 seconds).

Assuming this dependency, in Figure 8 we show the reverse shock afterglow emission superimposed on the  $\gamma$ -ray light-curve for the two different scenarios of gap production described in the above section. In Figure 8a we show the emission from a turned-off central source, while in Figure 8b we show the emission from a continuous modulated relativistic wind, both giving rise to a quiescent time of comparable duration in the  $\gamma$ -ray time history.

Clearly, since the width of the shell responsible for sweeping up the external medium varies by a factor of  $\Delta/\Delta_{\text{out}} = 7.5$  from one scenario to the other, one expects the reverse shock emission to peak 30 seconds earlier if the central engine turns off after six seconds. Furthermore, a second peak in the reverse shock emission may appear when the inner shell collide with the outer shell. This inner shell would then crash into the reverse shock, thermalizing its energy and boosting the power of the prompt afterglow. This second feature can be observed if the collision occurs before the reverse shock crosses the shell. It is worth noting that, while the prompt afterglow emission will be blueshifted in the EUV/soft X-ray bands if  $\rho_0 \gtrsim 10^4$  (see Eq. 10), the peak time  $t_p$  will not be strongly affected by the value of the density of the external medium ( $\Delta/c \gg t_{\text{dec}}$ , in this case).

We can thus conclude that the multiwavelength signature from the reverse shock emission, if measured, would be a clear way of determining whether or not the central engine turns off in order to produce a quiet period in the  $\gamma$ -ray time history.

#### 4 OBSERVED PROPERTIES OF QUIESCENT TIMES

In a previous work (Paper I) we have studied possible correlations between the duration of a quiescent time and that of the adjacent emission episodes. We have shown that a strong quantitative proportionality relation exists between the duration of an emission episode and the quiescent time

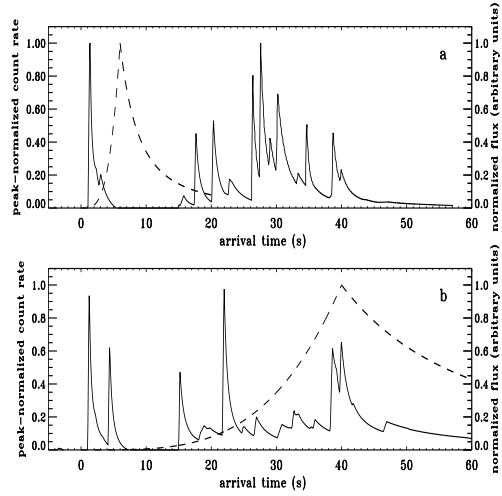


**Figure 8.** Light curves in two different energy bands for the two different scenarios described in figure 7. The solid curve is the main burst produced by internal shocks. The dashed line is the emission from the reverse shock. This emission terminates once the reverse shock crosses the shell and the cooling frequency drops below the observed frequency. During this period of emission one expects a  $\sim t^{-2}$  dependence. For a central engine that turns off (panel a), the emission from the reverse shock peaks much earlier than in the case of an engine in a steady state (panel b).

elapsed since the previous episode; while we found no clear correlation between the length of an emission episode and that of the following quiescent time.

In Paper I we outlined the general properties any dynamical system has to possess for it to show the observed correlation, under the hypothesis that the central engine turns off in correspondence to a quiescent time. Moreover, we envisaged that the mechanism responsible for extracting and dissipating the energy has to take place in a meta-stable configuration, such that the longer the accumulation period, the higher is the stored energy available for the next episode.

The hypothesis of an intermittent central engine, although intriguing, has to be tested against the observations. As we have demonstrated here, in the internal-external shock model, a modulation of the relativistic flow can produce quiescent times in the observed  $\gamma$ -ray lightcurve. Furthermore, a slow steady outflow ( $\Gamma_{\text{const}} < \Gamma_{\text{ave}}$ ), preceded and followed by a much faster, randomly modulated wind, could possibly be the origin of the observed correlation. As can be deduced from Figure 3d, if the time over which the source emits steadily is increased, the number of collisions with the later emitted shells (and the energy extracted from these collisions) will be larger. The whole energy contained in the steady outflow will be detected simultaneously or after the emission produced by the internal collisions between the following faster emitted shells.

It is thus reasonable to assume that the emission episode that follows a quiescent time produced in this manner will be more energetic. Nonetheless, the tight correlation we observe would require additional tuning of the parameters, as

the actual duration of the emission episode that follows a quiescent time is determined by the original duration of the emission at the inner engine and by the relative value of the Lorentz factor of the steady outflow.

In order to extract as much information as possible from the correlation, and to gain more insight into the dynamics of GRB central sources, we first need to better understand the physical processes responsible for the production of quiescent times in GRB light-curves. The fundamental question we would like to answer is whether the gaps are produced by a turning-off of the central engine or by a structure in the relativistic outflow velocity space.

In the former case, while it would be easy to account for the observed episodes of quiescence, we would need a model of the central engine able to go dormant for a period which is long compared to the typical dynamical timescale ( $\sim$  milliseconds) of the central source, and to be active again afterwards. Then, the observed correlation could be a clue to unveil the dynamical (and stability) properties of the system, as discussed in Paper I.

Alternatively, if the quiescent times are due to modulations of a relativistic wind that produces the  $\gamma$ -ray emission via internal shocks, they will instead probe the velocity structure of the outflow, and possibly its interaction with the ambient medium.

## 5 CONCLUSIONS

The very existence of quiescent times in GRB light-curves poses severe restrictions on the emission models. It is well known, for example, that in the external shock scenario it is almost impossible to reproduce this property (Fenimore & Ramirez-Ruiz 1999). In the internal shocks scenario the actual temporal profile is the outcome of the complex dynamics of the relativistic outflow, which has usually been considered as sequence of shells moving at different speeds. Within this framework, it is relatively easy to accommodate a large variety of GRB temporal profiles, given the large number of parameters on which the final observed light-curve depends.

The work we have presented here has been done with the aim of finding possible observational tests that could help us to discriminate between a turning-off of the central engine or a continuous relativistic outflow. We studied the various mechanisms that can produce a quiescent time in the internal shock model, and we have presented and discussed the results of a number of burst simulations. We conclude that, within such models, a central engine that goes dormant for a long enough period will always produce a quiescent time in the  $\gamma$ -ray light-curve of comparable duration. However, we have also shown that internal shocks can produce significant long periods of quiescence in the GRB light-curves without the central engine having to switch off. This can be achieved by an opportune modulation of a continuous relativistic wind. We discuss how different modulations could in principle be distinguished by studying the properties of burst light-curves in the X-ray and  $\gamma$ -ray energy bands (see Figs 4 and 6).

It is moreover possible to observationally determine whether the central engine turns off or not by analysing the multi-wavelength afterglow emission. In particular, we have shown that the peak of the prompt afterglow emis-

sion from the reverse shock strongly depends on whether the relativistic ejecta are part of a continuous wind or are instead made of a number of discrete thick shells, each one corresponding to an emission episode in the burst time history. To this end, a very rapid optical follow-up of the long bursts exhibiting periods of quiescence would be of the utmost importance, and could improve our understanding of the dynamical properties of  $\gamma$ -ray bursts progenitors.

## ACKNOWLEDGEMENTS

We thank P. Natarajan, A. Celotti, G. Morris and P. Madau for useful comments and suggestions. We are particularly grateful to E. E. Fenimore and P. Mészáros for very helpful insight regarding internal-shock calculations. ERR acknowledges support from CONACYT, SEP and the ORS foundation. AM thanks PPARC and the TMR network ‘Accretion onto black holes, compact stars and protostars’, funded by the European Commission under contract number ERBFMRX-CT98-0195, for support. MJR acknowledges support from the Royal Society.

## REFERENCES

- Akerlof, C. W., et al. 1999, *Nature*, 398, 400.  
 Blandford, R. D., & McKee, C. F., 1976, *Phys. Fluids*, 19, 1130.  
 Costa, E., et al. 1997, *Nature*, 387, 783.  
 Daigne, F., & Mochkovitch, R., 1998, *MNRAS*, 296, 275.  
 Fenimore, E. E., Cooper, C., Ramirez-Ruiz, E., Sumner, M. C., Yoshida, A. & Namiki, M., 1999, *ApJ*, 512, 683.  
 Fenimore, E. E. & Ramirez-Ruiz, E., 1999, *PASP Conf. Proc. Gamma-Ray Bursts: The First Three Minutes*, astro-ph/9906125  
 Fenimore, E. E. & Ramirez-Ruiz, E., 2000, to appear in *ApJ*, astro-ph/9909299.  
 Kobayashi, S., Piran, T., & Sari, R., 1997, *ApJ*, 490, 92.  
 Kouveliotou, C., et al., 1993, *ApJ*, 413, L101.  
 Kulkarni, S. R., et al., 1999, *Nature*, 398, 389.  
 Kumar, P. & Piran, T., 2000, *ApJ*, 532, 286.  
 Kuulkers et al., 2000, *ApJ*, 538, 638.  
 Lattimer, J. M., Schramm, D. N., 1976, *ApJ*, 210, 549.  
 MacFadyen, A. I., Woosley, S. E. & Heger, A., 1999, to appear in *ApJ*, astro-ph/9910034.  
 Mészáros, P., Laguna, P. & Rees, M. J. , 1993, *ApJ*, 415, 181.  
 Mészáros, P. & Rees, M. J. , 1997, *ApJ*, 476, 232.  
 Mészáros, P., Rees, M. J., Wijers, R., 1998, *ApJ*, 499, 301.  
 Mészáros, P. & Rees, M. J. , 1999, *MNRAS*, 306, L39.  
 Norris, J. P. et al., 1996, *ApJ*, 459, 2393.  
 Paczyński, B., 1998, *ApJ*, 494, L45.  
 Papathanassiou, H. & Mészáros, P., 1996, *ApJ*, 471, L91.  
 Ramirez-Ruiz, E. & Fenimore, E. E., 1999, *A&AS*, 138, 521.  
 Ramirez-Ruiz, E. & Fenimore, E. E., 2000, *ApJ*, 539, 712.  
 Ramirez-Ruiz, E. & Merloni, A., 2001, *MNRAS*, 320, L25 (Paper I).  
 Ramirez-Ruiz, E., Dray, L. M., Madau, P. & Tout, C., 2001, submitted to *MNRAS*, astro-ph/0012396.  
 Rees, M. J. & Mészáros, P., 1994, *ApJ*, 430, L93.  
 Rees, M. J., 1999, *A&AS*, 138, 491.  
 Sari, R. & Piran, T., 1997, *ApJ*, 485, 270.  
 Sari, R., 1997, *ApJ*, 489, L38.  
 Sari, R., Piran, T., & Narajan, R., 1998, *ApJ*, 497, L17.  
 Sari, R. & Piran, T., 1999, *ApJ*, 517, L109  
 Spada, M., Panaitescu, A. & Mészáros, P., 2000, *ApJ*, 537, 824.  
 van Paradijs et al, *Nature*, 386, 686, 1997.

This paper has been produced using the Royal Astronomical Society/Blackwell Science L<sup>A</sup>T<sub>E</sub>X style file.